Refereed Proceedings

The 13th International Conference on Fluidization - New Paradigm in Fluidization Engineering

Engineering Conferences International *Year* 2010

EXPERIMENTAL AND COMPUTATIONAL STUDY ON THE BUBBLE BEHAVIOR IN A 3-D FLUIDIZED BED WITH A VERTICAL-AXIS, ROTATING DISTRIBUTOR

Antonio Acosta Iborra* F. Hernández-Jiménez†

C. Sobrino‡ M. de Vega**

*University Carlos III of Madrid, aacosta@ing.uc3m.es

†Universidad Carlos III Madrid

‡Universidad Carlos III Madrid

**Universidad Carlos III Madrid

Experimental and computational study on the bubble behavior in a 3-D fluidized bed with a vertical-axis, rotating distributor

A. Acosta-Iborra, F. Hernández-Jiménez, C. Sobrino, M. de Vega
Universidad Carlos III Madrid, Avda. Universidad 30, 28911 Leganés, Madrid, Spain
T: 34-916248465; F: 34-916249430; E: aacosta@ing.uc3m.es

ABSTRACT

This work presents experimental measurements in a three-dimensional fluidized bed equipped with a novel vertical-axis, rotating distributor, together with two-fluid (Eulerian-Eulerian) CFD simulation results. The influence of the distributor rotation on the behavior of the bubbles in the experiments and in the CFD results is compared and critically analyzed.

INTRODUCTION

Different designs of air distribution have been proposed in the past as a way of improving the performance of gas solid fluidized beds (1, 2). Sobrino et al (3) experimentally studied the effect of a novel vertical-axis rotating distributor on the bubble characteristics in a bubbling fluidized bed, reporting smaller and more uniformly distributed bubbles than in the absence of rotation. The bubbles were detected and their sizes were measured using optical fiber probes, whose bubble characterization capabilities were compared previously (4) with the much more extensively employed pressure probes (5). In the present study, the three dimensional bed and the effect of the rotation of the distributor is simulated.

Simulation of medium and large scale gas fluidized beds is commonly undertaken by means of two-fluid computational fluid dynamic (CFD) models, also known as Eulerian-Eulerian two-phase models, which are primarily based on the representation of the gas phase and the particulate phase as two interpenetrating continua (6, 7). Two-fluid models provide information about the macroscopic hydrodynamics (i.e. velocity and volume fraction) of the two phases, including the bubble formation and motion. Therefore, these models are especially suitable for the understanding of the fluidized bed regarding dense phase bulk motion, and gas phase flow including bubbles. A greater detail in the description of the particle phase can be obtained using Lagrangian models such as Discrete Particle models (8) and Lattice Boltmann models (9), which allow the simulation of the individual motion of each particle. Although great progress has been done in the last few years in the field of Lagrangian models, their use is still restricted to a number of particles far below the amount encountered in fluidized beds of industrial interest.
There are several works comparing experimental results with two-fluid model computations of fluidized beds, especially in two-dimensional domains (see for example 10-14). These works reveal that two-fluid models can be used as an efficient tool for the understanding of the hydrodynamics of fluidized beds.
In the present study, a two-fluid (Eulerian-Eulerian) three-dimensional (3-D) CFD simulation of the bubbling fluidized bed with the rotating distributor is compared with experimental pressure and optical probe measurements. It should be noted that no

simulation of a 3-D fluidized bed with a vertical-axis rotating distributor has been previously reported in literature.

EXPERIMENTAL SET-UP

Experiments were carried out in a bubbling fluidized bed of 0.193 m internal diameter and 0.8 m height. The bed was filled with Geldart B silica sand particles with a mean diameter of 540 μm and a density of 2632.5 kg/m^3. The settled bed height was 22 cm. The column had a perforated plate to distribute the air through 90 holes of 2 mm diameter laid out in a hexagonal pitch of 15 mm. The total open area ratio of the distributor was 1%. The distributor could rotate around the vertical axis of the bed as it was coupled to an AC motor provided with an inverter, which allowed varying the rotational speed of the distributor from 0 to 100 rpm. Pressure and optical probes were introduced in the bed in order to detect the bubble passage along the axial and radial directions. The optical probes developed for the present study are based on backscattering principle, being their signal proportional to the particle volume fraction. The experimental set-up is represented in Figure 1, and its complete description can be found elsewhere (3).

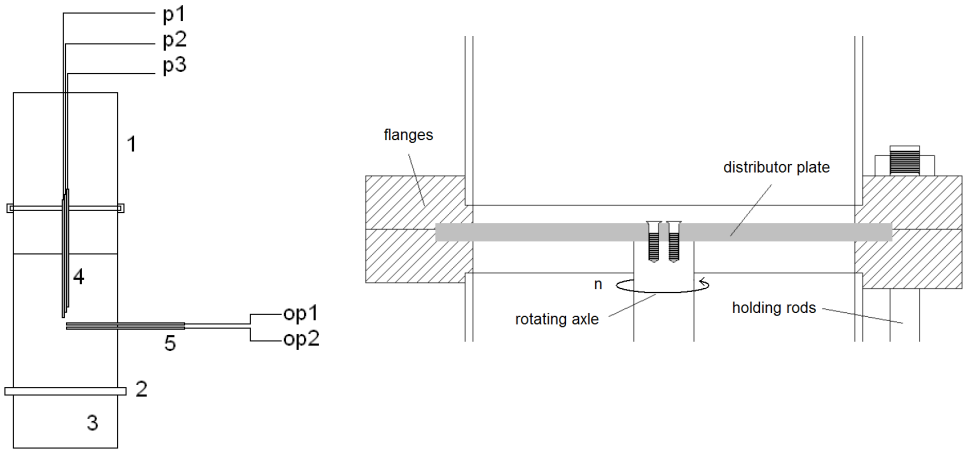

Figure 1: Left: Experimental set-up: 1) fluidized bed column 2) distributor plate 3) plenum chamber 4) pressure probes 5) optical probes. Right: detail of the rotating distributor assembly.

TWO-FLUID CFD MODEL

The CFD simulation of the fluidized bed with the novel vertical-axis, rotating distributor was performed using an Eulerian description of both the gas and particle phases by means of a Two-fluid model (6). This model is based on the approximation of the fluidized bed as two interpenetrating flows: a flow representing for the gas phase, and the other flow representing the particle phase treated as a continuum. In particular, the equations for the conservation of mass and momentum in the gas flow (g) and particulate flow (p) are (7):

$$\frac{\partial}{\partial t}\left(\varepsilon_g \rho_g\right)+\nabla\cdot\left(\varepsilon_g \rho_g \mathbf{v}_g\right)=0 \quad (1)$$

$$\frac{\partial}{\partial t}\left(\varepsilon_p \rho_p\right)+\nabla\cdot\left(\varepsilon_p \rho_p \mathbf{v}_p\right)=0 \quad (2)$$

$$\frac{\partial}{\partial t}\left(\varepsilon_g \rho_g \mathbf{v}_g\right)+\nabla\cdot\left(\varepsilon_g \rho_g \mathbf{v}_g \mathbf{v}_g\right)=-\varepsilon_g \nabla p+\nabla\cdot\left(\varepsilon_g \boldsymbol{\tau}_\mathbf{g}\right)-K_{gp}(v_g-v_p)+\varepsilon_g \rho_g \mathbf{g} \quad (3)$$

$$\frac{\partial}{\partial t}\left(\varepsilon_p \rho_p \mathbf{v}_p\right)+\nabla\cdot\left(\varepsilon_p \rho_p \mathbf{v}_p \mathbf{v}_p\right)=-\varepsilon_p \nabla p-\nabla p_p+\nabla\cdot\left(\varepsilon_p \boldsymbol{\tau}_p\right)+K_{gp}(v_g-v_p)+\varepsilon_p \rho_p \mathbf{g} \quad (4)$$

Where $\varepsilon_g+\varepsilon_p=1$ and $\tau_i=\mu_i(\nabla\mathbf{v}_i+\nabla\mathbf{v}_i{}^T)+\left(\lambda_i-\frac{2}{3}\mu_i\right)\left(\nabla\cdot\mathbf{v}_\mathbf{i}\right)\mathbf{I}$ for any phase "i", being the viscosity for the particulate phase composed of the collisional, kinematic and frictional viscosity $\mu_p=\mu_{p,col}+\mu_{p,kin}+\mu_{p,fr}$.

The mass and momentum equations are solved together with the differential equation for the transport of granular temperature Θ (7),

$$\frac{3}{2}\left[\frac{\partial}{\partial t}\left(\rho_p \varepsilon_p \Theta\right)+\nabla\cdot\left(\rho_p \varepsilon_p \Theta \mathbf{v}_\mathbf{p}\right)\right]=\left(-p_p\mathbf{I}+\boldsymbol{\tau}_p\right):\nabla\mathbf{v}_\mathbf{p}+\nabla\cdot\left(k_\Theta\nabla\cdot\Theta\right)-\gamma_\Theta \quad (5)$$

which is based on the kinetic theory of granular flows and provides the level of random fluctuation of particle velocity due to collisions. Notice that the granular temperature is required for the closure expressions of the drag coefficient K_{gp}, the solid viscosities μ_p and λ_p, and the effective particle pressure p_p. The diffusion coefficient of granular temperature k_Θ and the collision dissipation energy γ_Θ are also function of Θ. For the drag coefficient, the closure equation of Gidaspow et al (15) has been chosen due to its robustness at the beginning of the bubbling regime. Table 1 summarizes this and other closure models selected for the present study.

Table 1 Summary of closure models

Parameters	Closure model
K_{gp}, $\mu_{p,col}$, $\mu_{p,kin}$, k_Θ	Gidaspow et al (15)
$\mu_{p,fr}$	Schaeffer (16)
λ_p, p_p, γ_Θ	Lun et al (17)

The commercial CFD software Fluent 6.3 (18) was used for the solution of the system of equations (1) to (5) in a three-dimensional domain comprising all the interior volume of the cylinder where the fluidized bed is allocated. The dimensions of the cylinder are equal to the ones of the experimental rig. The domain was discretized with a structured mesh of 28800 hexahedral cells and 30805 nodes. The code discretized each of the equations with an implicit finite volume technique applied in any of the cells of the domain (19). Due to the great complexity and number of the equations involved, a larger amount of cells would lead to an inadmissible time of computation. However, to improve the spatial and temporal resolution of the solution, second order discretization in space and time was selected. After a sensitivity analysis of the solution, the chosen time step was equal to 2.5e-4 seconds with 40 iterations per time step together with an algebraic multigrid methodology for the solution of the implicit system equations (20). An effective value of the coefficient of restitution $e=0.9$ has been chosen to take into account not only the dissipation of kinetic energy due to inelastic deformation of

particles but also due to frictional losses (21). Other parameters of the simulation are shown in Table 2.

Table 2 Main parameters selected for the simulation

Parameter	Value	Parameter	Value
ρ_g [kg/m^3]	1.225	h_0 [m]	0.22
μ_g [Pa·s]	1.789e-5	U_g [m/s]	0.57
d_p [μm]	540	g [m/s^2]	9.81
ρ_p [kg/m^3]	2632.5	n [rpm]	0, 100
e []	0.9	Δt [s]	2.5e-4
$\varepsilon_{p,\max}$ []	0.555	N_i	40

Regarding the boundary conditions of the computational domain, the distributor was modeled as a porous plate placed at the base of the cylinder through which the flow air is injected into the fluidized bed. Particles are not allowed to cross the distributor. It has been assumed that gas and particles rotate with the same angular velocity as the distributor. This is fairly true for the case of the gas, as in the actual experimental rig the air has to cross the distributor and adopts its velocity. In the case of particles, it seems from the experiments that the particles placed close to the distributor have an angular velocity that approaches that of the distributor as the distance to the distributor diminishes. The rationale of this is probably related to the pressure of the dense phase, which tends to compress the particles towards the wall of the distributor. However, future studies have to prove the real extent to this hypothesis. The top of the cylinder is assumed to have a constant static pressure of one atmosphere, since it is opened to the exterior air. A no-slip condition for the gas flow was imposed at the lateral wall of the cylinder. For the dense phase flow, this condition is relaxed to non-penetration with negligible shear stresses at the lateral walls, since, in this kind of bed configuration, particles are well fluidized and do not remain attached to the wall.

RESULTS AND DISCUSSION

Pressure signals, taken from the experiment and the simulation for a representative period of time, are shown in figure 2 for the non-rotating case. In the same figure, optical probe measurements and simulated particle fractions are also plotted. The values depicted have been normalized. In the case of the differential pressure, the difference between pressures along the axis of the bed at heights z_1=12cm and z_2=13cm and divided by the mean value, is presented. The optical probe signal and the simulated particle fraction are also plotted relative to their mean value, at z=12cm. In each case we represent also the standard deviation of the data. As expected, the measured values have a slightly higher standard deviation, due to measurement errors. Both signals (differential pressure and particle fraction) present in any case a very similar behavior. The standard deviation of the differential pressure values (which is an indirect measure of the size of the bubble crossing the measurement point, as stated in (22)) compares well with the simulation results. Notice that the numerical results for the particle fraction can not overpass a pre-set limit of maximum agglomeration (0.56). This limit is not shown in the experimental results since the measured optical signal is subjected to a stochastic mixture of light scattering, reflection and blocking at high particle density, which also creates the high frequencies that superimpose over the bubble induced ones in the signal.

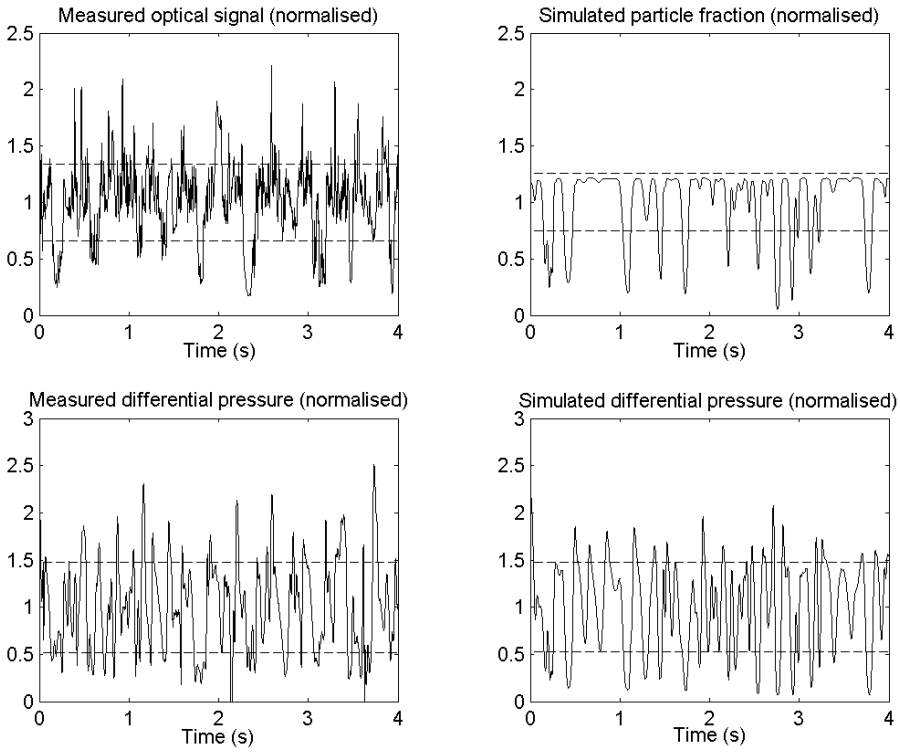

Figure 2: Measured (left) and simulated (right) signals at r/R=0.5. Up: particle fraction. Down: differential pressure obtained from pressure values at z_1=12cm and z_2=13cm. Dashed lines represent the standard deviation of the time series.

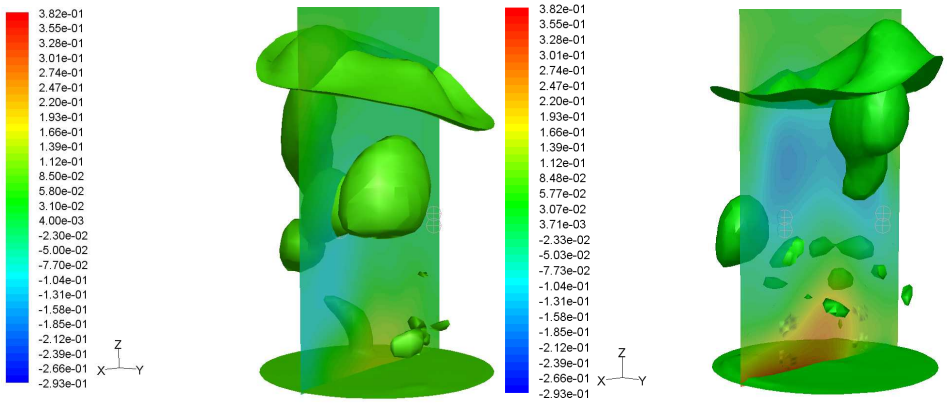

Figure 3: 3-D void distribution and contours of mean Y velocity of the particles in the plane y=0. Left: non-rotating distributor. Right: rotating distributor (100 rpm).

Figure 3 shows two snapshots of the instantaneous void distribution (bubbles) in the 3-D bed for the non-rotating ($n = 0\ rpm$) and rotating ($n = 100\ rpm$) cases obtained from the two-fluid model simulation. The bubbles have been obtained from iso-surfaces of void fraction equal to 0.7. There are visible voids in both configurations. In the case without rotation, larger void structures are generated. Besides, when the distributor rotates, a higher number of smaller voids can be distinguished. In the same figure, the mean Y particle velocity in the plane y=0 (vertical plane) is plotted. The particles present mainly an upflow through the center and a downflow near the

walls, in both cases. However, for the rotation case there is a higher particle motion in the Y-direction, which is more pronounced near the distributor.

The effect of the rotation in the bubble frequency is analyzed in figure-4 with the optical probe signal and the simulated solid void fraction for a point placed at the bed axis. In the case of the optical probe, the bubble passage is identified as a rapid voltage fall. The bubble detection threshold is determined as in (4) and (23). Bubbles detected following this threshold criterion are marked with a circle in figure 4, together with the horizontal line demarcating the voltage threshold value. A similar procedure is followed for the detection of a void in the simulation result.

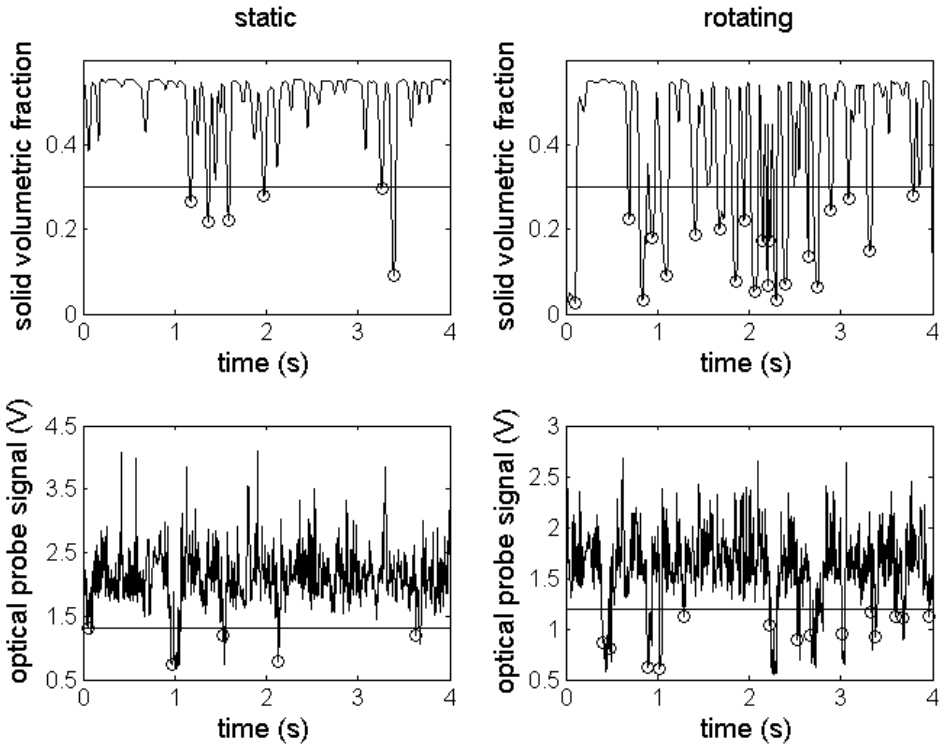

Figure 4: Simulated particle fraction (up) and optical probe signals (down) for the non-rotating case (left) and the distributor rotating at 100 rpm (right) distributor at the axis of the bed and separated a height z=10cm from the distributor.

As it can be observed, the bubble passage frequencies for the simulation and experimental results are of the same order. The effect of the distributor rotation is also similar in the experiments and the simulation: a higher frequency of bubble passage is observed when the distributor rotates. In particular, as Figure 4 shows, the rotation promotes a change from 5 (experiments) and 6 (simulation) bubbles in the non-rotating case to 14 (experiments) and 21 (simulation) bubbles in the rotating case. The resemblance is noteworthy taking into account the relatively short time-interval involved. A larger time interval, not simulated here owing to its great computational cost, would be necessary to obtain the Fourier spectra of the data. As the simulated distributor is a porous plate, it seems that this higher frequency of bubble passage is not merely due to a phenomenon related to the discontinuous character of the rotating distributor orifices, but may be related to a more complex hydrodynamic mechanism of the combined motion of the gas and particle phases that is induced during the distributor rotation.

CONCLUSIONS

Experimental measurements have been compared with two-phase CFD simulations of a three-dimensional fluidized bed with a vertical-axis, rotating distributor. Comparison of the simulated and measured pressure signals, as well as the simulated particle fraction and experimental optical probe signals, indicate reasonable agreement. Moreover, when the distributor rotates, the experimental and the simulated results provide also similar results: in both cases, a higher bubble passage frequency is observed. These results encourage the use of the two-fluid CFD simulation in future studies devoted to shed light into the underlying hydrodynamic mechanisms that promote a change in the bubble distribution when the distributor of the fluidized bed rotates.

NOTATION

d_p particle diameter, m
e restitution coefficient, dimensionless
g gravity acceleration, 9.81 m/s^2
h_0 static bed height, m
$\mathbf{I}$ unit tensor, dimensionless
k_Θ granular temperature diffusion coefficient, kg/m s
K_{gp} gas-particle momentum exchange coefficient, kg/m^3 s
N_i number of iteration per time step
p static pressure, Pa
U_g superficial gas velocity, m/s
$\mathbf{v}$ velocity vector, m/s

Greek letters

Δt time step, s
γ_Θ collision dissipation energy, kg/m s^3
ε volume fraction
Θ granular temperature, m^2/s^2
λ bulk viscosity, Pa·s
μ shear viscosity, Pa·s
ρ density, kg/m^3
$\boldsymbol{\tau}$ shear stress tensor, Pa
n rotational speed of the distributor, rpm

Subscripts

col collisional
fr frictional
g gas phase
kin kinematic
p particle phase
max maximum

REFERENCES

(1) F. Ouyang, O. Levenspiel, 1986. Spiral distributor for fluidized beds, Ind. Eng. Chem. Process Des. Dev., 25, pp. 504–507.
(2) C-S. Chyang and Y-C. Lin, 2002. A Study in the Swirling Fluidizing Pattern, J. Chem. Eng. Japan, 35, pp. 503-512.
(3) C. Sobrino, A. Acosta-Iborra, D. Santana and M. de Vega, 2009. Bubble characteristics in a bubbling fluidized bed with a rotating distributor, International Journal of Multiphase Flow, 35, pp. 970-976.
(4) C. Sobrino, J.A. Almendros-Ibáñez, D. Santana, C. Vázquez, M. de Vega, 2009. Maximum entropy estimation of the bubble size distribution in fluidized beds, 64, pp. 2307-2319.

(5) A.V. Ramayya, S.P. Venkateshan, A.K. Kolar, 1996. Estimation of bubble parameters from differential pressure measurements in gas-fluidized beds, 87, pp. 113-126.
(6) B. G. M. van Wachem, A. E. Almstedt, 2003. Methods for multiphase computational fluid dynamics. Chem. Eng. J. 96, pp 81-98.
(7) D. Gidaspow. Multiphase Flow and Fluidization. Academic Press, Boston, 1994.
(8) N. G. Deen, M. Van Sint Annaland, M. A. Van der Hoef, J. A. M. Kuipers, 2007. Review of discrete particle modelling of fluidized beds Chem. Eng. Sci. 62, pp. 28-44.
(9) A.J.C. Ladd, and R. Verberg, 2001. Lattice-Boltzmann simulations of particle fluid suspensions. J. of Statistical Physics 104, pp. 1191-1251.
(10) T. McKeen, T. Pugsley, 2003. Simulation and experimental validation of a freely bubbling bed of FCC catalyst. Powder Technology 129, pp. 139-152.
(11) F. Taghipour, N. Ellis, C. Wong, 2005. Experimental and computacional study of gas-solid fluidized bed hydrodynamics. Chem. Eng. Sci. 60, pp. 6857-6867.
(12) A. Busciglio, G. Vella, G. Micale, L. Rizzuti, 2009. Analysis of the bubbling behaviour of 2D gas solid fluidized beds: Part II. Comparison between experiments and numerical simulation via Digital Image Analysis Technique. Chem. Eng. J. 148, pp.145-163.
(13) E. Peirano, V. Delloume, B. Leckner, 2001. Two- or three-dimensional simulations of turbulent gas–solid flows applied to fluidization. Chem. Eng. Sci. 56, pp. 4787– 4799.
(14) N. Xie, F. Battaglia, S. Pannala, 2008. Effects of using two- versus three-dimensional computational modeling of fluidized beds. Part I, hydrodynamics. Powder Technology 182, pp. 1-13.
(15) D. Gidaspow, R. Bezburuah, and J. Ding, 1992. Hydrodynamics of Circulating Fluidized Beds, Kinetic Theory Approach. In: Fluidization VII, Proceedings of the 7th Engineering Foundation Conference on Fluidization, pp 75-82.
(16) D. G. Schaeffer, 1987. Instability in the Evolution Equations Describing Incompressible Granular Flow. J. Diff. Eq. 66, pp.19-50.
(17) C. K. K. Lun, S. B. Savage, D. J. Jeffrey, and N. Chepurniy, 1984. Kinetic Theories for Granular Flow: Inelastic Particles in Couette Flow and Slightly Inelastic Particles in a General Flow Field. J. Fluid Mech. 140, pp 223-256.
(18) Fluent Inc. 2006. Fluent 6.3 User's Guide. http://www.fluent.com
(19) S. V. Patankar Numerical Heat Transfer and Fluid Flow. Taylor & Francis. 1980.
(20) B. R. Hutchinson and G. D. Raithby, 1986. A Multigrid Method Based on the Additive Correction Strategy. Numerical Heat Transfer 9, pp. 511-537.
(21) M. J. V. Goldschmidt, J. A. Kuipers, W. P. M. van Swaaij, 2001. Hydrodynamic modelling of dense gas-fluidised beds using the kinetic theory of granular flow: effect of coefficient of restitution on bed dynamics. Chem. Eng. Sci. 56, pp. 571-578.
(22) J. van der Schaaf, J.C. Schouten, F. Johnsson, C.M. van den Bleek, 2002. Non-intrusive determination of bubble and slug length scales in fluidized beds by decomposition of the power spectral density of pressure time series. International Journal of Multiphase Flow 28, 865-880.
(23) J-M. Schweitzer, J. Bayle, T. Gauthier, 2001. Local gas hold-up measurements in fuidized bed and slurry bubble column, Chemical Engineering Science, 56, pp. 1103-1110.